Intensity interferometry for ultralight bosonic dark matter detection

Hector Masia-Roig[1,2,*] Nataniel L. Figueroa[1,2,†] Ariday Bordon[1,2,‡] Joseph A. Smiga[1,2] Yevgeny V. Stadnik[3]
Dmitry Budker[1,2,4] Gary P. Centers[1,2] Alexander V. Gramolin[5] Paul S. Hamilton[6] Sami Khamis[6]
Christopher A. Palm[7] Szymon Pustelny[8] Alexander O. Sushkov[5,9,10] Arne Wickenbrock[1,2] and Derek F. Jackson Kimball[7,§]

[1]*Johannes Gutenberg-Universität Mainz, 55128 Mainz, Germany*
[2]*Helmholtz-Institut Mainz, GSI Helmholtzzentrum für Schwerionenforschung, 55128 Mainz, Germany*
[3]*School of Physics, The University of Sydney, New South Wales 2006, Australia*
[4]*Department of Physics, University of California at Berkeley, Berkeley, California 94720-7300, USA*
[5]*Department of Physics, Boston University, Boston, Massachusetts 02215, USA*
[6]*Department of Physics and Astronomy, University of California, Los Angeles, California 90095, USA*
[7]*Department of Physics, California State University—East Bay, Hayward, California 94542-3084, USA*
[8]*Institute of Physics, Jagiellonian University, 30-059 Kraków, Poland*
[9]*Department of Electrical and Computer Engineering, Boston University, Boston, Massachusetts 02215, USA*
[10]*Photonics Center, Boston University, Boston, Massachusetts 02215, USA*

Ultralight bosonic dark matter (UBDM) can be described by a classical wavelike field oscillating near the Compton frequency of the bosons. If a measurement scheme for the direct detection of UBDM interactions is sensitive to a signature quadratic in the field, then there is a near-zero-frequency (dc) component of the signal. Thus, a detector with a given finite bandwidth can be used to search for bosons with Compton frequencies many orders of magnitude larger than its bandwidth. This opens the possibility of a detection scheme analogous to Hanbury Brown and Twiss intensity interferometry. Assuming that the UBDM is virialized in the Galactic gravitational potential, the random velocities produce slight deviations from the Compton frequency. These result in stochastic fluctuations of the intensity on a timescale determined by the spread in kinetic energies. In order to mitigate ubiquitous local low-frequency noise, a network of sensors can be used to search for the stochastic intensity fluctuations by measuring cross-correlation between the sensors. This method is inherently broadband, since a large range of Compton frequencies will yield near-zero-frequency components within the sensor bandwidth that can be searched for simultaneously. Measurements with existing sensor networks have sufficient sensitivity to search experimentally unexplored parameter space.

I. INTRODUCTION

A wide variety of evidence suggests the existence of dark matter, an invisible substance that constitutes a large fraction of the matter in the Universe [1–3]. Despite decades of research, its microscopic nature remains unknown. A promising hypothesis is that dark matter predominantly consists of ultralight bosons with masses $m_\varphi \ll 1$ eV/c^2, such as axions [4–6], axionlike particles

*hemasiar@uni-mainz.de
†figueroa@uni-mainz.de
‡aridaybordon@gmail.com
§derek.jacksonkimball@csueastbay.edu

(ALPs) [7,8], or hidden photons [9–11]. Ultralight bosons can couple to Standard Model (SM) particles through a variety of "portals" [12,13], which have been used to search for ultralight bosonic dark matter (UBDM)—see, for example, Refs. [14–31].

Numerous experiments looking for UBDM are based on resonant systems, which require accurate tuning to the unknown Compton frequency, $\omega_c = m_\varphi c^2/\hbar$, in order to be sensitive to UBDM. Therefore, a time-consuming scan of tunable parameters must be performed to search a wide range of masses. However, if a search is based on the measurement of the "intensity" of the UBDM, part of the signal is down-converted to near-zero frequency [32,33], regardless of the particular Compton frequency of the UBDM.

In the commonly considered simplest version of the standard halo model (SHM) for dark matter [34–36], the net UBDM field results from the superposition of numerous virialized bosons [37]. Such a model assumes minimal

self-interactions [38] and ignores possible nonvirialized dark matter streams [39] and composite dark matter structures, such as boson stars [40] or topological defects [41]. The velocity dispersion of the dark matter particles in the neighborhood of our solar system is $v_0 \sim 10^{-3}c$. Consequently, the oscillation frequencies associated with the virialized bosons are Doppler shifted. This generates a fractional shift from ω_c and a spread of frequencies of $\sim v_0^2/(2c^2) \sim 5 \times 10^{-7}$. Because of the random distribution of frequencies of the UBDM, the amplitude of the net UBDM field stochastically fluctuates, as discussed in detail in Refs. [42–49]. We emphasize that this is an essential feature of the UBDM field in the SHM. The characteristic timescale $\tau_\varphi \sim 2\hbar/(m_\varphi v_0^2)$ and length scale $\lambda_\varphi \sim \hbar/(m_\varphi v_0)$ of the fluctuations depend on the mass m_φ and velocity dispersion v_0 of the bosons [37]. In comparison to a direct measurement of the UBDM field, a measurement of the UBDM field intensity produces a frequency down-conversion of the UBDM signal to near dc. The spectral linewidth of this near-dc signal is $\sim 10^6$ times smaller than ω_c. Looking for this near-dc feature allows sensors with a limited bandwidth to probe UBDM with masses $\sim 10^6$ times larger than searching for direct field oscillations at ω_c.

The frequency down-conversion discussed above occurs naturally when considering quadratic portals where the interaction with SM particles is proportional to the square of the UBDM field [32,33,41,50–53]. A spin-0 field $\varphi(\mathbf{r}, t)$ can interact with SM fermions and electromagnetic fields according to the phenomenological quadratic scalar Lagrangian [32]

$$\mathcal{L}_s = \hbar c \left(\pm \frac{m_f c^2}{\Lambda_f^2} \bar{\psi}_f \psi_f \pm \frac{1}{4\Lambda_\gamma^2} F_{\mu\nu}^2 \right) \varphi^2(\mathbf{r}, t), \quad (1)$$

where Λ_f and Λ_γ parametrize the couplings to fermions and photons, respectively, where the $\pm$ indicates the sign of the coupling, m_f is the fermion mass, ψ_f is the fermion field, and $F_{\mu\nu}$ is the Faraday tensor.

The effects of the interactions described by Eq. (1) can be understood in terms of redefinitions of the effective fermion masses and the fine-structure constant α [32,50],

$$m_f^{(\text{eff})}(\mathbf{r}, t) = m_f \left(1 \mp \frac{\hbar c}{\Lambda_f^2} \varphi^2(\mathbf{r}, t) \right), \quad (2)$$

$$\alpha^{(\text{eff})}(\mathbf{r}, t) = \alpha \left(1 \pm \frac{\hbar c}{\Lambda_\gamma^2} \varphi^2(\mathbf{r}, t) \right). \quad (3)$$

Variations of $m_f^{(\text{eff})}$ and $\alpha^{(\text{eff})}$ can be measured with atomic clocks or interferometers [50,52–62], or generally by direct comparison of systems with different dependence on these fundamental constants [28,63–66].

Additionally, a spin-0 pseudoscalar (ALP) field can possess linear and/or quadratic interactions with the axial-vector current of a SM fermion [41], $\bar{\psi}_f \gamma^\mu \gamma_5 \psi_f$,

$$\mathcal{L}_{\text{lin}} = \pm \frac{1}{f_l} \bar{\psi}_f \gamma^\mu \gamma_5 \psi_f \partial_\mu \varphi(\mathbf{r}, t), \quad (4)$$

$$\mathcal{L}_{\text{quad}} = \pm \frac{1}{f_q^2} \bar{\psi}_f \gamma^\mu \gamma_5 \psi_f \partial_\mu \varphi^2(\mathbf{r}, t), \quad (5)$$

where f_l and f_q parametrize the linear and quadratic couplings to fermion spins, and γ^μ and γ_5 are Dirac matrices. The quantum chromodynamics (QCD) axion [67–71] associated with the Peccei-Quinn solution to the strong *CP* problem [72] generally possesses the linear coupling described by Eq. (4) (see, for example, Ref. [73]). Alternatively, in effective field theories with ALPs not associated with the QCD sector, the linear coupling term may be strongly suppressed or absent [51], in which case the leading-order interaction with the axial-vector current may be the quadratic coupling of Eq. (5) [41]. Note that, like Eq. (4), the description of the quadratic interaction in Eq. (5) is manifestly Lorentz covariant, since replacing φ by φ^2 preserves the overall number-type Lorentz structure because φ is a spinless field. Effective field theories featuring an ALP-spin interaction dominated by the quadratic term have much weaker constraints on the associated coupling constant f_q from astrophysics [41,51]. Of note is the fact that, while the linear interaction of Eq. (4) is *CP* conserving, the quadratic interaction in Eq. (5) is *CP* violating, and thus could potentially play a role in baryogenesis [74]. While models with interactions $\propto \varphi^2$ were originally developed phenomenologically (see Ref. [51] and references therein), string theory is an example of a fundamental theory generating quadratic interactions [75] such as those described by Eqs. (1) and (5), and theoretical work in this area is ongoing. Since our proposed search method relies on signals quadratic in the ALP field, in the rest of this work we focus our attention on the quadratic coupling.

In the nonrelativistic limit, Eq. (5) yields the interaction Hamiltonian [41,53]

$$\mathcal{H}_\varphi = \mp \frac{2\hbar^2 c^2}{f_q^2} \mathbf{S} \cdot \boldsymbol{\nabla}\varphi^2(\mathbf{r}, t). \quad (6)$$

Equation (6) features a structure similar to that of the Zeeman Hamiltonian, $\mathcal{H}_Z = \gamma \mathbf{S} \cdot \mathbf{B}$, where γ is the gyromagnetic ratio and $\mathbf{B}$ is a magnetic field (with the above noted difference that $\mathcal{H}_Z$ is *CP* even, while $\mathcal{H}_\varphi$ is *CP* odd). Therefore, $\boldsymbol{\nabla}\varphi^2(\mathbf{r}, t)$ couples to a fermion spin $\mathbf{S}$ in a manner similar to a magnetic field [41], playing the role of a "pseudomagnetic" field. Thus, such pseudoscalar fields can be searched for in the spin dynamics of electrons or nuclei. While a variety of sensors could be used, here we focus on

atomic (nuclear) magnetometers since these are intrinsically sensitive to Zeeman shifts [76–82].

The effects described by Eqs. (2), (3), and (6) are related to φ^2, which is in turn proportional to the UBDM intensity and exhibit near-dc stochastic amplitude fluctuations. Although measuring low-frequency signals is technically challenging due to multiple sources of low-frequency noise, an array of independent, geographically distributed sensors will tend to have uncorrelated noise. In contrast, the slowly changing UBDM intensity will lead to a common-mode fluctuating signal present in all detectors within a coherence length of one another, which will appear in correlations between the sensors. We advocate for the use of networks of sensors to search for these stochastic fluctuations. There are existing and proposed dark matter searches sensitive to these interactions using networks consisting of a variety of sensor types, such as atomic clocks [50,53–56,83], atomic magnetometers [41,76–80,84–86], gravimeters [87–89], laser interferometers [52,57,58,60–62,90], and atom interferometers [59]. The methodology described below is analogous to Hanbury Brown and Twiss intensity interferometry [91] and can be used to dramatically expand the range of UBDM Compton frequencies that particular sensors can probe [92].

II. STOCHASTIC PROPERTIES OF THE UBDM FIELD

The properties of the UBDM field can be derived using the framework described in Refs. [37,42–49]. In brief, assuming that UBDM does not interact with itself, each individual particle can be treated as an independent wave. In this scenario, the UBDM field is well described by a superposition of these individual waves.

Assuming that the local dark-matter energy density $\rho_{\rm dm}$ is solely in the form of UBDM, such field can be modeled as the superposition of N oscillators,[1]

$$\varphi(\mathbf{r}, t) \approx \sum_{n=1}^{N} \frac{\varphi_0}{\sqrt{N}} \cos(\omega_n t - \mathbf{k}_n \cdot \mathbf{r} + \theta_n), \qquad (7)$$

where the oscillation amplitude is given by [73]

$$\varphi_0 = \frac{\hbar}{m_\varphi c} \sqrt{2\rho_{\rm dm}}, \qquad (8)$$

such that the average energy density in the UBDM field comprises the totality of the local dark matter. Here, $\mathbf{k}_n = m_\varphi \mathbf{v}_n / \hbar$ is the wave vector corresponding to

---

[1]The individual bosons should be modeled as quantum objects, not classical fields. However, the huge occupancy numbers of each mode allows one to accurately model the UBDM as a superposition of classical oscillators. For example, a boson mass of 10^{-11} eV/c^2 (and $\rho_{\rm dm} = 0.3$ GeV/cm^3) results in a number density of particles of $\sim 10^{19}$ cm^3. The de Broglie wavelength for particles moving with v_0 is $\sim 10^{10}$ cm.

$\mathbf{v}_n$, the velocity of the nth oscillator in the laboratory frame. The phases θ_n are randomly distributed between 0 and 2π. The oscillation frequency ω_n is determined mostly by the Compton frequency ω_c of the underlying ultralight boson. The kinetic energy correction to the rest energy introduces small deviations from ω_c, so that

$$\omega_n \approx \omega_c \left(1 + \frac{\mathbf{v}_n^2}{2c^2} \right), \qquad (9)$$

for $v_n \ll c$. Therefore, the distribution of ω_n (and $\mathbf{k}_n$) is determined by the velocity distribution as observed in the laboratory frame. According to the standard halo model, $\mathbf{v}_n$ follows a displaced Maxwell-Boltzmann distribution defined as

$$f_{\rm lab}(\mathbf{v}) \approx \frac{1}{\pi^{3/2} v_0^3} \exp\left(-\frac{(\mathbf{v} - \mathbf{v}_{\rm lab})^2}{v_0^2} \right), \qquad (10)$$

where the velocity of the lab frame is $\mathbf{v}_{\rm lab} = |\mathbf{v}_{\rm lab}|\hat{\mathbf{z}}$, and we have ignored the escape-velocity cutoff.

Sufficiently strong self-interactions could introduce effects in the coherence properties of the UBDM field not considered in this work. However, since these interactions are expected to be relatively weak [38,44], they are commonly neglected in studies of direct detection searches [37,48,93], as in this work. Here, our interest lies in quadratic interactions with the field, proportional to $\varphi^2(\mathbf{r}, t)$ or $\nabla\varphi^2(\mathbf{r}, t)$. These quantities have two terms: one near-dc and one fast oscillating component at $\approx 2\omega_c$. We consider sensors with a limited bandwidth $\Delta\omega \ll \omega_c$, such that the fast oscillating terms can be ignored. Therefore, only the near-dc components (denoted by the subscript s) of φ^2 and $\nabla\varphi^2$ are considered. These are written as

$$\varphi_s^2(\mathbf{r}, t) = \frac{\varphi_0^2}{2N} \sum_{n,m=1}^{N} \cos(\omega_{nm}t - \mathbf{k}_{nm} \cdot \mathbf{r} + \theta_{nm}), \qquad (11)$$

$$\nabla\varphi_s^2(\mathbf{r}, t) = \frac{\varphi_0^2}{2N} \sum_{n,m=1}^{N} \mathbf{k}_{nm} \sin(\omega_{nm}t - \mathbf{k}_{nm} \cdot \mathbf{r} + \theta_{nm}), \qquad (12)$$

where $\omega_{nm} = \omega_n - \omega_m$, $\mathbf{k}_{nm} = \mathbf{k}_n - \mathbf{k}_m$, and $\theta_{nm} = \theta_n - \theta_m$. Since the sensors are assumed to be within the same coherence patch (such that $\Delta\mathbf{k} \cdot \Delta\mathbf{r} \approx 0$, where $\Delta\mathbf{k}$ is the characteristic spread of values in $\mathbf{k}_{nm}$ and $\Delta\mathbf{r}$ is the difference in the position vectors for the pair of sensors at $\mathbf{r}_n$ and $\mathbf{r}_m$), the $\mathbf{r}$ dependence can be neglected and we can evaluate the expressions at $\mathbf{r} = 0$ in the following calculations [94].

The signal measured with each sensor would have a small UBDM-related component $\kappa\xi(t)$, where κ accounts for the coupling of the sensor to the UBDM field, and $\xi(t)$ is either φ_s^2 (scalar interaction) or $\hat{\mathbf{m}} \cdot \nabla\varphi_s^2$ (pseudoscalar gradient interaction, where $\hat{\mathbf{m}}$ represents the sensitive direction of the sensor). The correlations between measurable signals produced in different sensors by a UBDM

field can be quantified using the degree of first-order coherence $g^{(1)}(\tau)$ for different delay times τ,

$$g^{(1)}(\tau) = \frac{\langle \xi(t)\xi(t+\tau) \rangle_t}{\langle \xi^2 \rangle_t}, \tag{13}$$

where $\langle \cdots \rangle_t$ denotes the time average. The value of $g^{(1)}(\tau)$ is a measure of the degree of correlation between $\xi(t)$ and $\xi(t+\tau)$.

To illustrate the stochastic properties of $\nabla\varphi_s^2(0,t)$ and $\varphi_s^2(0,t)$, their time evolution was simulated. Plots of $g^{(1)}(\tau)$ for $\varphi_s^2(t)$ and for projections of $\nabla\varphi_s^2(t)$ onto parallel and perpendicular directions with respect to $\boldsymbol{v}_{\text{lab}}$ can be seen in Fig. 1. In order to numerically calculate the near-dc components of φ^2 and $\nabla\varphi_s^2(t)$, and avoid the double summation in Eq. (12), it is convenient to introduce the field in complex notation,

$$\varphi_c(0,t) = \frac{\varphi_0}{\sqrt{N}} \sum_{n=1}^{N} \exp\left[i(\omega_n t + \theta_n)\right]. \tag{14}$$

Then the near-dc component of the field squared can be calculated using

$$\varphi_s^2 = \frac{1}{2}\varphi_c\varphi_c^*. \tag{15}$$

This yields a real number related to the average value of φ^2 over a cycle of the oscillation.

Similarly, $\nabla\varphi_s^2$ is numerically evaluated by applying the chain rule

$$\nabla\varphi_s^2(\boldsymbol{r},t)|_{\boldsymbol{r}=0} = \frac{i}{2}\varphi_c \frac{\varphi_0}{\sqrt{N}} \sum_{n=1}^{N} \boldsymbol{k}_n \exp[-i(\omega_n t + \theta_n)]$$
$$-\frac{i}{2}\varphi_c^* \frac{\varphi_0}{\sqrt{N}} \sum_{n=1}^{N} \boldsymbol{k}_n \exp\left[i(\omega_n t + \theta_n)\right]. \tag{16}$$
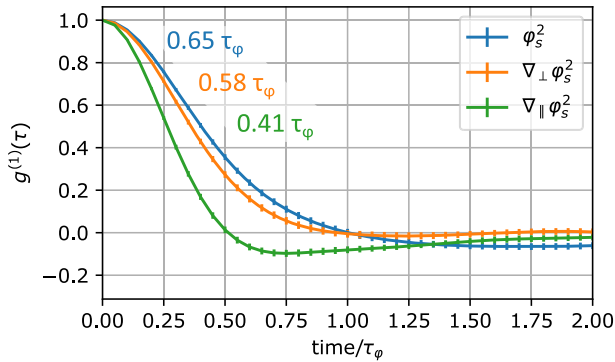

FIG. 1. Degree of first-order coherence as a function of delay time τ for φ_s^2 and different projections of the gradient $\nabla\varphi_s^2$ relative to $\boldsymbol{v}_{\text{lab}}$. Each curve is the result of 100 averages simulating 10^3 particles, where the mean was subtracted. The approximate values of the coherence times are given in colors matching their respective plot traces.

Note that by first evaluating Eq. (14) to obtain $\varphi_c(0,t)$ and then evaluating Eqs. (15) and (16) to find φ_s^2 and $\nabla\varphi_s^2$, we only evaluate sums with $\mathcal{O}(N)$ terms for N oscillators. This is in contrast to the equivalent expressions presented in Eqs. (11) and (12), which have double sums with $\mathcal{O}(N^2)$ terms. This makes numerical calculations using Eqs. (15) and (16) considerably faster for large N.

The individual wave vectors $\boldsymbol{k}_n$ and frequencies ω_n are calculated from the velocities $\boldsymbol{v}_n$. These velocities are drawn from the displaced Maxwell-Boltzmann distribution defined in Eq. (10). In our simulations, we take the isotropic velocity dispersion of the local UBDM to be determined by the characteristic virial velocity $v_0 \approx 220$ km/s and $\boldsymbol{v}_{\text{lab}}$ to be dominated by the motion of the Sun in the Galactic frame, $|\boldsymbol{v}_{\text{lab}}| \approx 233$ km/s. The phases θ_n are drawn from a uniform distribution spanning from 0 to 2π.

The simulations consider $N = 10^3$ oscillators evolving during $20\tau_\varphi$ with a time resolution of $0.05\tau_\varphi$, where τ_φ is calculated using Eq. (18). The number of oscillators used to model the UBDM field reflects the quantity that can be comfortably simulated with our available hardware. By repeating the simulation hundreds of times, we observe that the results converge. Additional checks confirmed that the spectral properties of the simulations matched theoretical predictions. For example, an analytical solution for $g^{(1)}(\tau)$ in the limit $|\boldsymbol{v}_{\text{lab}}| \gg v_0$ can be found in the Supplemental Material, Sec. D [97], which is shown to agree with our simulations. The temporal resolution and the duration of the simulated field evolution were chosen considering plausible values for an experimental search.

After generating φ_s^2 and $\nabla\varphi_s^2$, $g^{(1)}(\tau)$ is calculated using Eq. (13). Note that the mean value of the field is subtracted so $g^{(1)}(\tau) \to 0$ for $\tau \gg \tau_\varphi$ (see the Supplemental Material, Sec. B [97]).

The coherence time τ_c is the characteristic time after which the correlation in the UBDM field is lost. We define the coherence time as the power-equivalent width of $g^{(1)}(\tau)$ [98,99],

$$\tau_c = \int_{-\infty}^{+\infty} |g^{(1)}(\tau)|^2 d\tau, \tag{17}$$

which describes a characteristic temporal width of $g^{(1)}(\tau)$. We used this expression to quantify the coherence time in our simulations.[2]

As a useful benchmark to compare our results with, we have used the coherence time τ_φ of the field assuming an exact Lorentzian line shape (with a full width at half maximum of $\omega_c v_0^2/c^2$) [37,49],

---

[2]For the simulations presented here, the coherence time was obtained by integrating Eq. (17) numerically. The integration was done over the time interval $[0, 5\tau_\varphi]$ and multiplying by 2 in order to account for the negative segment of the range.

$$\tau_\varphi \approx \frac{2\hbar}{m_\varphi v_0^2}. \tag{18}$$

Because the actual spectral line shape describing φ is non-Lorentzian [49], the coherence time of the field φ derived from the simulations differs from τ_φ. For the considered $\mathbf{v}_{\text{lab}}$, simulations show a coherence time of $\approx 1.12(1)\tau_\varphi$.

The coherence time for φ_s^2 is approximately half of that for the field φ. This is a result of the field φ_s^2 being a sum over terms depending on the difference of frequencies ω_{nm}, as opposed to φ, which only contains terms depending on ω_n. The probability distribution of ω_{nm} can be calculated as the convolution of the distribution of ω_n with itself. This results in a distribution for ω_{nm} that is broader. Consequently, the coherence time is shorter since $g^{(1)}(\tau)$ is given by the Fourier transform of the power spectral density of φ_s^2 (proportional to the ω_{nm} distribution), according to the Wiener-Khinchin theorem. The gradient coupling features even shorter coherence times due to the $\mathbf{k}_{nm}$ factor weighting the contribution of the oscillating terms. Larger ω_{nm} tends to correspond to larger $\mathbf{k}_{nm}$: this effectively broadens the power spectral density of $\nabla \varphi_s^2$, leading to a shorter coherence time. This is also the reason why parallel and perpendicular components of the gradient have different coherence times, as discussed below.

The coherence time is also related to the mass of the UBDM particle, as can be seen in Eq. (18). The relationship between the UBDM mass and the coherence time exhibited by φ_s^2 and $\nabla \varphi_s^2$ is shown in Fig. 2. The coherence times for φ_s^2 and $\nabla \varphi_s^2$ are proportional to the coherence time of φ, τ_φ as defined in Eq. (18). In the case of detection, this could be used to estimate the mass of the UBDM particles.

A possible method to look for UBDM is to use multisensor intensity interferometry to measure the cross-correlation between time-series data from different sensors. When using pairs of geographically distributed sensors, a correlated global background field will produce a nonzero cross-correlation $g_{AB}^{(1)}(\tau)$ between sensors A and B
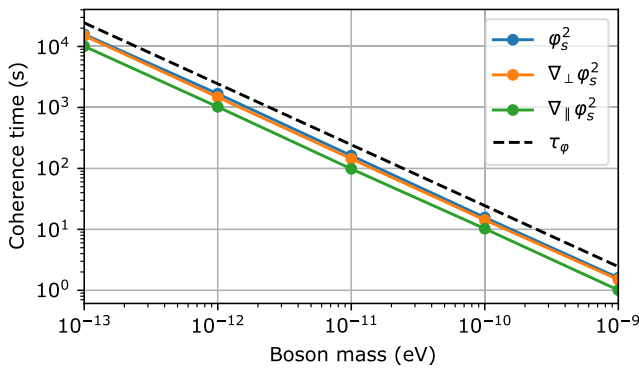

FIG. 2. Mass dependence of the coherence time τ_c for φ_s^2 and projections of $\nabla \varphi_s^2$. Each point is the result of 100 averages simulating 10^3 particles.

proportional to $g^{(1)}(\tau)$, as discussed in the Supplemental Material, Sec. B [97]. Note that uncorrelated noise in the sensors will reduce the expected value of $g_{AB}^{(1)}(0)$ in the presence of a UBDM signal, making it smaller than the maximum value of one (see the Supplemental Material, Sec. B [97]). In the case of the gradient coupling, a relative misalignment of the sensitive axes of the sensors also leads to a reduction in the value of $g_{AB}^{(1)}(0)$ (see the Supplemental Material, Sec. C [97]). In order to distinguish a correlated signal from uncorrelated noise, $g_{AB}^{(1)}(0)$ can be compared with $g_{AB}^{(1)}(\tau \gg \tau_\varphi)$.

III. ACCESSIBLE UBDM PARAMETER SPACE

Existing sensor networks have sufficient sensitivity to probe experimentally unexplored parameter space describing UBDM by searching for correlated stochastic fluctuations using intensity interferometry.

Atomic magnetometers can search for ALP fields by detecting Zeeman shifts caused by the interaction described in Eq. (6). In analogy with the Zeeman Hamiltonian, the gradient of the square of the ALP field acts as a pseudo-magnetic field $\mathcal{B}_q$ given by

$$\mathcal{B}_q \approx \mp \frac{2\hbar^2 c^2}{g_F \mu_B f_q^2} \nabla \varphi^2(\mathbf{r}, t), \tag{19}$$

where g_F is the Landé factor, and μ_B is the Bohr magneton (or, for nuclear-spin-based magnetometers, the nuclear magneton). The projection of the near-dc component of $\mathcal{B}_q$ along the sensitive axis of a magnetometer defined by the unit vector $\hat{\mathbf{m}}$ can be estimated in a manner similar to that discussed in, for example, Ref. [49], by evaluating the sum in Eq. (12), yielding a characteristic magnitude (with an average value of zero) of

$$\hat{\mathbf{m}} \cdot \mathcal{B}_q \sim \frac{\hbar^3 \rho_{\text{dm}} v_0}{g_F \mu_B m_\varphi f_q^2}. \tag{20}$$

In the derivation of the above equation, we assumed that frequency and wave vector are uncorrelated. The accuracy of this approximation is discussed in the Supplemental Material, Sec. A [97]. Nonetheless, Eq. (20) is suitable for a rough estimate of the sensitivity of a magnetometer network to such UBDM, given that $|\mathbf{v}_{\text{lab}}| \approx v_0$.

The sensitivity of a sensor network depending on the number of sensors (N_m), the UBDM field coherence time (τ_φ), and total acquisition time (T) is discussed in the Supplemental Material, Sec. B [97]. Combining Eqs. (20) and (B6), an estimate for the UBDM coupling constant to which a magnetometer network would be sensitive is given by
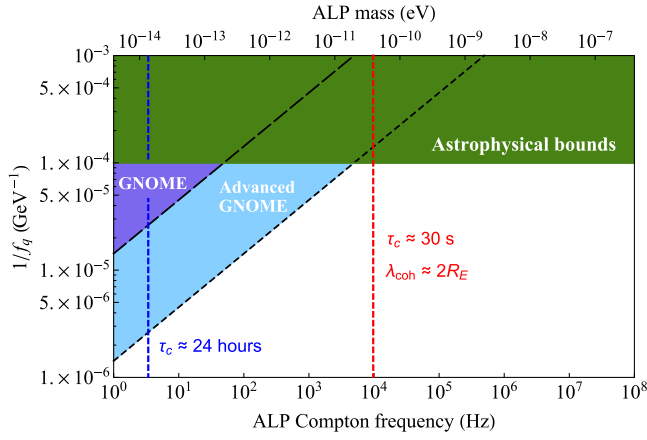
FIG. 3. Estimated parameter space describing ALP dark matter that can be probed by GNOME (dashed line, purple shaded region) and Advanced GNOME (dotted line, light blue shaded region) measuring for ≈ 100 days using $N_m = 10$ magnetometers [76,77,80,82]. GNOME and Advanced GNOME are sensitive to the interaction of the ALP field with proton spins described by Eq. (6); f_q parametrizes the ALP-nucleon coupling strength. The vertical dashed red line marks the Compton frequency and mass for which the ALP coherence length equals the Earth's diameter. The vertical dashed blue line marks the Compton frequency and mass for which $\tau_c \approx 24$ h. The dark red shaded region shows constraints from the NASDUCK experiment [100]. The dark green shaded area represents astrophysical bounds on spin-dependent ALP interactions with nucleons [51,101]. Note, however, that there are theoretical scenarios where these astrophysical bounds can be circumvented [102].

$$f_q^2 \lesssim \frac{\hbar^3 \rho_{\mathrm{dm}} v_0}{g_F \mu_B m_\varphi \delta B} (\tau_\varphi T)^{1/4} \sqrt{N_m}. \qquad (21)$$

Figure 3 shows sensitivity estimates for the global network of optical magnetometers for exotic physics searches (GNOME) [76,77,80,82] based on alkali vapor magnetometers with $\delta B \approx 100$ fT/$\sqrt{\mathrm{Hz}}$ and the Advanced GNOME network based on noble gas comagnetometers with $\delta B \approx 1$ fT/$\sqrt{\mathrm{Hz}}$, assuming $T = 100$ days and $N_m = 10$. Note that for $\tau_c \gg 24$ h, the signal amplitude is partially modulated at the frequency of Earth's rotation since the signals are $\propto \hat{m} \cdot \mathcal{B}_q$ and $\hat{m}$ rotates with the Earth, while $\mathcal{B}_q$ does not, which can in principle enable the detection of UBDM with coherence times much longer than a day. Notable is the extent to which GNOME and Advanced GNOME can probe UBDM with Compton frequencies far beyond the nominal sensor bandwidths.

Optical atomic clocks are an example of a sensor that can search for scalar fields through the apparent variation of fundamental constants as described in Eqs. (2) and (3), due to, for example, the variation of the fine-structure constant α and relativistic effects (see Ref. [13] and references therein). For example, the fractional frequency variation in an atomic

clock due to variation of the fine-structure constant α is given by

$$\frac{\delta\nu(t)}{\nu} = \kappa_\alpha \frac{\delta\alpha(t)}{\alpha}, \qquad (22)$$

where ν is the clock frequency and κ_α is a dimensionless sensitivity coefficient that depends on the type of clock: $\kappa_\alpha \approx 2$ for most current optical atomic clocks, but note that there are exceptions, such as the proposed clock with $\kappa_\alpha \approx -15$ described in Ref. [104], and the possibility of future clocks based on highly charged ions [105] or a thorium nuclear transition [106] that could have orders of magnitude larger values of κ_α.

It is important to note that the sensitivity of intensity interferometry can be significantly impacted by backaction of the surrounding matter density on the scalar field as pointed out in Refs. [33,107] and also discussed in Refs. [51,108,109]. The accessible range of parameter space for current optical clocks near the surface of Earth is well within the regime where such backaction effects are significant (above the long-dashed blue line in Fig. 4, see the Supplemental Material, Sec. E [97]). However, for the range of boson masses and coupling constants considered in the present work, it turns out that for a space-based
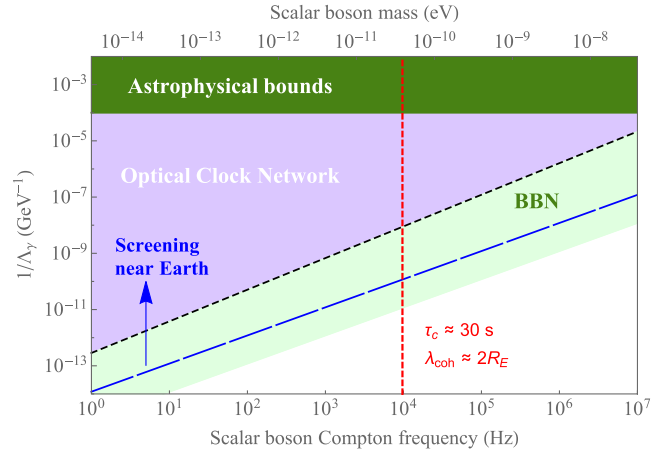

FIG. 4. Estimated parameter space describing UBDM fields that can be probed by an optical clock network such as those described in Refs. [83,103] (dotted line, light purple shaded region) in ≈ 100 days of searching for correlated stochastic fluctuations using $N_c = 10$ clocks, not accounting for (anti) screening from backaction [33,107], which can play a significant role near Earth's surface above the long-dashed blue line as indicated by the blue arrow. Clocks are sensitive to the interactions described by Eq. (1); Λ_γ parametrizes the strength of the coupling of the ultralight bosons to photons. The vertical dashed red line marks the Compton frequency and mass for which the ultralight boson's coherence length equals the Earth's diameter. The dark green shaded area represents astrophysical bounds on such quadratic scalar interactions between ultralight bosons and photons from stellar cooling and observations of supernova 1987a [51,101]; the light green shaded region represents bounds from big bang nucleosynthesis (BBN) [32].

network of sensors [110] the screening effects can be largely neglected [107], and so, for simplicity, we consider such a space-based network in our sensitivity estimates.

Assuming the effect described by Eq. (3) and a scalar field that makes up the entirety of the dark matter density, the amplitude of the fractional frequency variation is given by

$$\frac{\delta \nu}{\nu} \approx \kappa_\alpha \frac{2\hbar^3 \rho_{\mathrm{dm}}}{\Lambda_\gamma^2 m_\varphi^2 c}. \tag{23}$$

Optical clock networks, with N_c independent clocks, can achieve a fractional frequency uncertainty [83,103]

$$\frac{\delta \nu}{\nu} \approx \frac{3 \times 10^{-16}}{(\tau_\varphi T)^{1/4} \sqrt{N_c}}, \tag{24}$$

which translates to the sensitivity to the quadratic scalar coupling constant shown in Fig. 4. The Supplemental Material, Sec. F [97] offers a heuristic argument for the significant sensitivity difference between atomic clock and magnetometer networks to the respective coupling parameters Λ_γ and f_q.

IV. CONCLUSION

In summary, we propose a new method to search for UBDM by using intensity interferometry with sensor networks. We show that, when the sensors measure signals quadratic in the UBDM field, there is a near-dc component of the signal that enables finite-bandwidth sensors to search for UBDM with Compton frequencies many orders of magnitude larger than possible if a traditional search for signals oscillating at the Compton frequency is carried out. Here we have focused on quadratic UBDM interactions and sensors with a linear response; however, the results are also valid for linear interactions and sensors that respond quadratically to the field (square-law detectors). The method of intensity interferometry is intrinsically broadband, with the potential to search for UBDM with particle masses ranging over many orders of magnitude without having to probe individual narrow frequency bands. UBDM searches with intensity interferometry using existing sensor networks can probe unexplored parameter space.

[1] J. L. Feng, Dark matter candidates from particle physics and methods of detection, Annu. Rev. Astron. Astrophys. **48**, 495 (2010).

[2] David N. Spergel, The dark side of cosmology: Dark matter and dark energy, Science **347**, 1100 (2015).

[3] Peter W. Graham, Igor G. Irastorza, Steven K. Lamoreaux, Axel Lindner, and Karl A. van Bibber, Experimental searches for the axion and axion-like particles, Annu. Rev. Nucl. Part. Sci. **65**, 485 (2015).

[4] J. Preskill, M. B. Wise, and F. Wilczek, Cosmology of the invisible axion, Phys. Lett. **120B**, 127 (1983).

[5] L. F. Abbott and P. Sikivie, A cosmological bound on the invisible axion, Phys. Lett. **120B**, 133 (1983).

[6] M. Dine and W. Fischler, The not-so-harmless axion, Phys. Lett. **120B**, 137 (1983).

[7] P. W. Graham, D. E. Kaplan, and S. Rajendran, Cosmological Relaxation of the Electroweak Scale, Phys. Rev. Lett. **115**, 221801 (2015).

[8] Raymond T. Co, Lawrence J. Hall, and Keisuke Harigaya, Predictions for axion couplings from ALP cogenesis, J. High Energy Phys. 01 (2021) 172.

[9] Bob Holdom, Two U(1)'s and epsilon charge shifts, Phys. Lett. **166B**, 196 (1986).

[10] Mirjam Cvetič and Paul Langacker, Implications of Abelian extended gauge structures from string models, Phys. Rev. D **54**, 3570 (1996).

[11] L. B. Okun, Limits of electrodynamics: Paraphotons?, Sov. Phys. JETP **56**, 502 (1982), http://jetp.ras.ru/cgi-bin/dn/e_056_03_0502.pdf.

[12] Peter W. Graham, David E. Kaplan, Jeremy Mardon, Surjeet Rajendran, and William A. Terrano, Dark matter direct detection with accelerometers, Phys. Rev. D **93**, 075029 (2016).

[13] M. S. Safronova, D. Budker, D. DeMille, Derek F. Jackson Kimball, A. Derevianko, and Charles W. Clark, Search for new physics with atoms and molecules, Rev. Mod. Phys. **90**, 025008 (2018).

[14] S. Asztalos, E. Daw, H. Peng, L. J. Rosenberg, C. Hagmann, D. Kinion, W. Stoeffl, K. van Bibber, P. Sikivie, N. S. Sullivan, D. B. Tanner, F. Nezrick, M. S. Turner, D. M. Moltz, J. Powell, M.-O. André, J. Clarke, M. Mück, and Richard F. Bradley, Large-scale microwave cavity search for dark-matter axions, Phys. Rev. D **64**, 092003 (2001).

[15] S. J. Asztalos, G. Carosi, C. Hagmann, D. Kinion, K. van Bibber, M. Hotz, L. J. Rosenberg, G. Rybka, J. Hoskins, J. Hwang, P. Sikivie, D. B. Tanner, R. Bradley, and J. Clarke, Squid-Based Microwave Cavity Search for Dark-Matter Axions, Phys. Rev. Lett. **104**, 041301 (2010).

[16] Dmitry Budker, Peter W. Graham, Micah Ledbetter, Surjeet Rajendran, and Alexander O. Sushkov, Proposal for a Cosmic Axion Spin Precession Experiment (CASPEr), Phys. Rev. X **4**, 021030 (2014).

[17] P. Sikivie, N. Sullivan, and D. B. Tanner, Proposal for Axion Dark Matter Detection Using an *LC* Circuit, Phys. Rev. Lett. **112**, 131301 (2014).

[18] Saptarshi Chaudhuri, Peter W. Graham, Kent Irwin, Jeremy Mardon, Surjeet Rajendran, and Yue Zhao, Radio for hidden-photon dark matter detection, Phys. Rev. D **92**, 075012 (2015).

[19] Andrew A. Geraci and Andrei Derevianko, Sensitivity of Atom Interferometry to Ultralight Scalar Field Dark Matter, Phys. Rev. Lett. **117**, 261301 (2016).

[20] Christopher Abel, Nicholas J. Ayres, Giles Ban, Georg Bison, Kazimierz Bodek, V. Bondar, Manfred Daum, Malcolm Fairbairn, Victor V. Flambaum, Peter Geltenbort *et al.*, Search for Axionlike Dark Matter through Nuclear Spin Precession in Electric and Magnetic Fields, Phys. Rev. X **7**, 041034 (2017).

[21] Teng Wu, John W. Blanchard, Gary P. Centers, Nataniel L. Figueroa, Antoine Garcon, Peter W. Graham, Derek F. Jackson Kimball, Surjeet Rajendran, Yevgeny V. Stadnik, Alexander O. Sushkov *et al.*, Search for Axionlike Dark Matter with a Liquid-State Nuclear Spin Comagnetometer, Phys. Rev. Lett. **122**, 191302 (2019).

[22] Antoine Garcon, John W. Blanchard, Gary P. Centers, Nataniel L. Figueroa, Peter W. Graham, Derek F. Jackson Kimball, Surjeet Rajendran, Alexander O. Sushkov, Yevgeny V. Stadnik, Arne Wickenbrock *et al.*, Constraints on bosonic dark matter from ultralow-field nuclear magnetic resonance, Sci. Adv. **5**, eaax4539 (2019).

[23] Arran Phipps, S. E. Kuenstner, S. Chaudhuri, C. S. Dawson, B. A. Young, C. T. FitzGerald, H. Froland, K. Wells, D. Li, H. M. Cho *et al.*, Exclusion limits on hidden-photon dark matter near 2 neV from a fixed-frequency superconducting lumped-element resonator, in *Microwave Cavities and Detectors for Axion Research* (Springer, New York, 2020), p. 139.

[24] Jack Manley, Dalziel J. Wilson, Russell Stump, Daniel Grin, and Swati Singh, Searching for Scalar Dark Matter with Compact Mechanical Resonators, Phys. Rev. Lett. **124**, 151301 (2020).

[25] N. Crescini, D. Alesini, C. Braggio, G. Carugno, D. DAgostino, D. Di Gioacchino, P. Falferi, U. Gambardella, C. Gatti, G. Iannone *et al.*, Axion Search with a Quantum-Limited Ferromagnetic Haloscope, Phys. Rev. Lett. **124**, 171801 (2020).

[26] T. Braine, R. Cervantes, N. Crisosto, N. Du, S. Kimes, L. J. Rosenberg, G. Rybka, J. Yang, D. Bowring, A. S. Chou *et al.*, Extended Search for the Invisible Axion with the Axion Dark Matter Experiment, Phys. Rev. Lett. **124**, 101303 (2020).

[27] K. M. Backes, D. A. Palken, S. Al Kenany, B. M. Brubaker, S. B. Cahn, A. Droster, Gene C. Hilton, Sumita Ghosh, H. Jackson, S. K. Lamoreaux *et al.*, A quantum enhanced search for dark matter axions, Nature (London) **590**, 238 (2021).

[28] Dionysios Antypas, Oleg Tretiak, Ke Zhang, Antoine Garcon, Gilad Perez, Mikhail G. Kozlov, Stephan Schiller, and Dmitry Budker, Probing fast oscillating scalar dark matter with atoms and molecules, Quantum Sci. Technol. **6**, 034001 (2021).

[29] Tanya S. Roussy, Daniel A. Palken, William B. Cairncross, Benjamin M. Brubaker, Daniel N. Gresh, Matt Grau, Kevin C. Cossel, Kia Boon Ng, Yuval Shagam, Yan Zhou *et al.*, Experimental Constraint on Axionlike Particles over Seven Orders of Magnitude in Mass, Phys. Rev. Lett. **126**, 171301 (2021).

[30] Deniz Aybas *et al.*, Search for Axionlike Dark Matter Using Solid-State Nuclear Magnetic Resonance, Phys. Rev. Lett. **126**, 141802 (2021).

[31] Alexander V Gramolin, Deniz Aybas, Dorian Johnson, Janos Adam, and Alexander O. Sushkov, Search for axion-like dark matter with ferromagnets, Nat. Phys. **17**, 79 (2021).

[32] Y. V. Stadnik and V. V. Flambaum, Can Dark Matter Induce Cosmological Evolution of the Fundamental Constants of Nature?, Phys. Rev. Lett. **115**, 201301 (2015).

[33] Aurélien Hees, Olivier Minazzoli, Etienne Savalle, Yevgeny V. Stadnik, and Peter Wolf, Violation of the equivalence principle from light scalar dark matter, Phys. Rev. D **98**, 064051 (2018).

[34] P. A. Zyla *et al.*, Review of particle physics, Prog. Theor. Exp. Phys. **2020**, 083C01 (2020), and 2021 update.

[35] N. Wyn Evans, Ciaran A. J. O'Hare, and Christopher McCabe, Refinement of the standard halo model for dark matter searches in light of the Gaia Sausage, Phys. Rev. D **99**, 023012 (2019).

[36] Andrzej K. Drukier, Katherine Freese, and David N. Spergel, Detecting cold dark-matter candidates, Phys. Rev. D **33**, 3495 (1986).

[37] Andrei Derevianko, Detecting dark-matter waves with a network of precision-measurement tools, Phys. Rev. A **97**, 042506 (2018).

[38] Bohua Li, Tanja Rindler-Daller, and Paul R. Shapiro, Cosmological constraints on Bose-Einstein-condensed scalar field dark matter, Phys. Rev. D **89**, 083536 (2014).

[39] Jürg Diemand, Michael Kuhlen, Piero Madau, M. Zemp, Ben Moore, D. Potter, and J. Stadel, Clumps and streams in the local dark matter distribution, Nature (London) **454**, 735 (2008).

[40] Joshua Eby, Chris Kouvaris, Niklas Grønlund Nielsen, and L. C. R. Wijewardhana, Boson stars from self-interacting dark matter, J. High Energy Phys. 02 (2016) 028.

[41] M. Pospelov, S. Pustelny, M. P. Ledbetter, D. F. Jackson Kimball, W. Gawlik, and D. Budker, Detecting Domain Walls of Axionlike Models Using Terrestrial Experiments, Phys. Rev. Lett. **110**, 021803 (2013).

[42] G. P. Centers, J. W. Blanchard, J. Conrad, N. L. Figueroa, A. Garcon, A. V. Gramolin, D. F. Jackson Kimball, M. Lawson, B. Pelssers, J. A. Smiga, A. O. Sushkov, A. Wickenbrock, D. Budker, and A. Derevianko, Stochastic fluctuations of bosonic dark matter, Nat. Commun. **12**, 7321 (2021).

[43] J. W. Foster, N. L. Rodd, and B. R. Safdi, Revealing the dark matter halo with axion direct detection, Phys. Rev. D **97**, 123006 (2018).

[44] Lam Hui, Wave dark matter, Annu. Rev. Astron. Astrophys. **59**, 247 (2021).

[45] Hsi-Yu Schive, Tzihong Chiueh, and Tom Broadhurst, Cosmic structure as the quantum interference of a coherent dark wave, Nat. Phys. **10**, 496 (2014).

[46] Michael S. Turner, Periodic signatures for the detection of cosmic axions, Phys. Rev. D **42**, 3572 (1990).

[47] Ciaran A. J. O'Hare and Anne M. Green, Axion astronomy with microwave cavity experiments, Phys. Rev. D **95**, 063017 (2017).

[48] Mariangela Lisanti, Matthew Moschella, and William Terrano, Stochastic properties of ultralight scalar field gradients, Phys. Rev. D **104**, 055037 (2021).

[49] Alexander V. Gramolin, Arne Wickenbrock, Deniz Aybas, Hendrik Bekker, Dmitry Budker, Gary P. Centers, Nataniel L. Figueroa, Derek F. Jackson Kimball, and Alexander O. Sushkov, Spectral signatures of axionlike dark matter, Phys. Rev. D **105**, 035029 (2022).

[50] A. Derevianko and M. Pospelov, Hunting for topological dark matter with atomic clocks, Nat. Phys. **10**, 933 (2014).

[51] K. A. Olive and M. Pospelov, Environmental dependence of masses and coupling constants, Phys. Rev. D **77**, 043524 (2008).

[52] Y. V. Stadnik and V. V. Flambaum, Searching for Dark Matter and Variation of Fundamental Constants with Laser and Maser Interferometry, Phys. Rev. Lett. **114**, 161301 (2015).

[53] Conner Dailey, Colin Bradley, Derek F Jackson Kimball, Ibrahim A Sulai, Szymon Pustelny, Arne Wickenbrock, and Andrei Derevianko, Quantum sensor networks as exotic field telescopes for multi-messenger astronomy, Nat. Astron. **5**, 150 (2021).

[54] P. Wcisło, P. Morzyński, M. Bober, A. Cygan, D. Lisak, R. Ciuryło, and M. Zawada, Experimental constraint on dark matter detection with optical atomic clocks, Nat. Astron. **1**, 0009 (2016).

[55] Benjamin M. Roberts, Geoffrey Blewitt, Conner Dailey, Mac Murphy, Maxim Pospelov, Alex Rollings, Jeff Sherman, Wyatt Williams, and Andrei Derevianko, Search for domain wall dark matter with atomic clocks on board global positioning system satellites, Nat. Commun. **8**, 1 (2017).

[56] Benjamin M. Roberts, Pacome Delva, Ali Al-Masoudi, Anne Amy-Klein, Christian Baerentsen, C. F. A. Baynham, Erik Benkler, Slawomir Bilicki, Sebastien Bize, William Bowden *et al.*, Search for transient variations of the fine structure constant and dark matter using fiber-linked optical atomic clocks, New J. Phys. **22**, 093010 (2020).

[57] Koji Nagano, Tomohiro Fujita, Yuta Michimura, and Ippei Obata, Axion Dark Matter Search with Interferometric Gravitational Wave Detectors, Phys. Rev. Lett. **123**, 111301 (2019).

[58] Lorenzo Aiello, Jonathan W. Richardson, Sander M. Vermeulen, Hartmut Grote, Craig Hogan, Ohkyung Kwon, and Chris Stoughton, Constraints on Scalar Field Dark Matter from Colocated Michelson Interferometers, Phys. Rev. Lett. **128**, 121101 (2022).

[59] L. Badurina, E. Bentine, Diego Blas, K. Bongs, D. Bortoletto, T. Bowcock, K. Bridges, W. Bowden, O. Buchmueller, C. Burrage *et al.*, Aion: An atom interferometer observatory and network, J. Cosmol. Astropart. Phys. 05 (2020) 011.

[60] Y. V. Stadnik and V. V. Flambaum, Enhanced effects of variation of the fundamental constants in laser interferometers and application to dark-matter detection, Phys. Rev. A **93**, 063630 (2016).

[61] H. Grote and Y. V. Stadnik, Novel signatures of dark matter in laser-interferometric gravitational-wave detectors, Phys. Rev. Res. **1**, 033187 (2019).

[62] Sander M. Vermeulen *et al.*, Direct limits for scalar field dark matter from a gravitational-wave detector, Nature (London) **600**, 424 (2021).

[63] D. Antypas, O. Tretiak, A. Garcon, R. Ozeri, G. Perez, and D. Budker, Scalar Dark Matter in the Radio-Frequency Band: Atomic-Spectroscopy Search Results, Phys. Rev. Lett. **123**, 141102 (2019).

[64] Dionysios Antypas, Dmitry Budker, Victor V. Flambaum, Mikhail G. Kozlov, Gilad Perez, and Jun Ye, Fast apparent oscillations of fundamental constants, Ann. Phys. (Amsterdam) **532**, 1900566 (2020).

[65] R. Oswald, A. Nevsky, V. Vogt, S. Schiller, N. L. Figueroa, K. Zhang, O. Tretiak, D. Antypas, D. Budker, A. Banerjee, and G. Perez, Search for Dark-Matter-Induced Oscillations of Fundamental Constants Using Molecular Spectroscopy, Phys. Rev. Lett. **129**, 031302 (2022).

[66] Oleg Tretiak, Xue Zhang, Nataniel L. Figueroa, Dionysios Antypas, Andrea Brogna, Abhishek Banerjee, Gilad Perez, and Dmitry Budker, Improved Bounds on Ultralight Scalar

Dark Matter in the Radio-Frequency Range, Phys. Rev. Lett. **129,** 031301 (2022).

[67] Jihn E. Kim, Weak-Interaction Singlet and Strong CP Invariance, Phys. Rev. Lett. **43,** 103 (1979).

[68] M. A. Shifman, A. I. Vainshtein, and V. I. Zakharov, Can confinement ensure natural *CP* invariance of strong interactions?, Nucl. Phys. **B166,** 493 (1980).

[69] A. R. Zhitnitsky, On possible suppression of the axion hadron interactions. (In Russian), Yad. Fiz. **31,** 497 (1980); [Sov. J. Nucl. Phys. **31,** 260 (1980)].

[70] Michael Dine, Willy Fischler, and Mark Srednicki, A simple solution to the strong *CP* problem with a harmless axion, Phys. Lett. **104B,** 199 (1981).

[71] P. Sikivie, Experimental Tests of the "Invisible" Axion, Phys. Rev. Lett. **51,** 1415 (1983).

[72] Roberto D. Peccei and Helen R. Quinn, *CP* Conservation in the Presence of Instantons, Phys. Rev. Lett. **38,** 1440 (1977).

[73] P. W. Graham and S. Rajendran, New observables for direct detection of axion dark matter, Phys. Rev. D **88,** 035023 (2013).

[74] Werner Bernreuther, *CP* violation and baryogenesis, in *CP Violation in Particle, Nuclear and Astrophysics* (Springer, New York, 2002), pp. 237–293.

[75] Kurt Hinterbichler, Justin Khoury, and Horatiu Nastase, Towards a uv completion of chameleons in string theory, J. High Energy Phys. 03 (2011) 061.

[76] S. Pustelny, D. F. Jackson Kimball, C. Pankow, M. P. Ledbetter, P. Wlodarczyk, P. Wcislo, M. Pospelov, J. R. Smith, J. Read, W. Gawlik, and D. Budker, The global network of optical magnetometers for exotic physics (GNOME): A novel scheme to search for physics beyond the standard model, Ann. Phys. (Berlin) **525,** 659 (2013).

[77] S. Afach, Dmitry Budker, G. DeCamp, Vincent Dumont, Zoran Dragan Grujić, H. Guo, D. F. Jackson Kimball, T. W. Kornack, Victor Lebedev, W. Li *et al.*, Characterization of the global network of optical magnetometers to search for exotic physics (GNOME), Phys. Dark Universe **22,** 162 (2018).

[78] D. F. Jackson Kimball, D. Budker, J. Eby, M. Pospelov, Szymon Pustelny, Theo Scholtes, Y. V. Stadnik, Antoine Weis, and A. Wickenbrock, Searching for axion stars and Q-balls with a terrestrial magnetometer network, Phys. Rev. D **97,** 043002 (2018).

[79] Hector Masia-Roig, Joseph A. Smiga, Dmitry Budker, Vincent Dumont, Zoran Grujic, Dongok Kim, Derek F. Jackson Kimball, Victor Lebedev, Madeline Monroy, Szymon Pustelny, Theo Scholtes, Perrin C. Segura, Yannis K. Semertzidis, Yun Chang Shin, Jason E. Stalnaker, Ibrahim Sulai, Antoine Weis, and Arne Wickenbrock, Analysis method for detecting topological defect dark matter with a global magnetometer network, Phys. Dark Universe **28,** 100494 (2020).

[80] Samer Afach, Ben C. Buchler, Dmitry Budker, Conner Dailey, Andrei Derevianko, Vincent Dumont, Nataniel L. Figueroa, Ilja Gerhardt, Zoran D. Grujić, Hong Guo *et al.*, Search for topological defect dark matter with a global network of optical magnetometers, Nat. Phys. **17,** 1396 (2021).

[81] Min Jiang, Haowen Su, Antoine Garcon, Xinhua Peng, and Dmitry Budker, Search for axion-like dark matter with spin-based amplifiers—Nature Physics, Nat. Phys. **17,** 1402 (2021).

[82] S. Afach, D. Aybas Tumturk, H. Bekker, B. C. Buchler, D. Budker, K. Cervantes, A. Derevianko, J. Eby, N. L. Figueroa, R. Folman *et al.*, What can a GNOME do? Search targets for the global network of optical magnetometers for exotic physics searches, arXiv:2305.01785.

[83] Boulder Atomic Clock Optical Network BACON Collaboration, Frequency ratio measurements at 18-digit accuracy using an optical clock network, Nature (London) **591,** 564 (2021).

[84] Michael A. Fedderke, Peter W. Graham, Derek F. Jackson Kimball, and Saarik Kalia, The Earth as a transducer for dark-photon dark-matter detection, Phys. Rev. D **104,** 075023 (2021).

[85] Michael A. Fedderke, Peter W. Graham, Derek F. Jackson Kimball, and Saarik Kalia, Search for dark-photon dark matter in the supermag geomagnetic field dataset, Phys. Rev. D **104,** 095032 (2021).

[86] Ariel Arza, Michael A. Fedderke, Peter W. Graham, Derek F. Jackson Kimball, and Saarik Kalia, Earth as a transducer for axion dark-matter detection, Phys. Rev. D **105,** 095007 (2022).

[87] Wenxiang Hu, Matthew M. Lawson, Dmitry Budker, Nataniel L. Figueroa, Derek F. Jackson Kimball, Allen P. Mills, and Christian Voigt, A network of superconducting gravimeters as a detector of matter with feeble non-gravitational coupling, Eur. Phys. J. D **74,** 115 (2020).

[88] Rees L. McNally and Tanya Zelevinsky, Constraining domain wall dark matter with a network of superconducting gravimeters and LIGO, Eur. Phys. J. D **74,** 1 (2020).

[89] Charles J. Horowitz and R. Widmer-Schnidrig, Gravimeter Search for Compact Dark Matter Objects Moving in the Earth, Phys. Rev. Lett. **124,** 051102 (2020).

[90] Evan D. Hall, Rana X. Adhikari, Valery V. Frolov, Holger Müller, and Maxim Pospelov, Laser interferometers as dark matter detectors, Phys. Rev. D **98,** 083019 (2018).

[91] R. Hanbury Brown and R. Q. Twiss, The question of correlation between photons in coherent light rays, Nature (London) **178,** 1447 (1956).

[92] Note that, although Refs. [37,93] consider UBDM interferometry using sensor networks, they do not consider the intensity interferometry as we do here.

[93] J. W. Foster, Y. Kahn, R. Nguyen, N. L. Rodd, and B. R. Safdi, Dark matter interferometry, Phys. Rev. D **103,** 076018 (2021).

[94] Note that the spatial dependence for coherence lengths smaller than Earth's diameter could also be exploited to look for UBDM, for which portable sensors could be employed, as in Refs. [95,96].

[95] Jacopo Grotti, Silvio Koller, Stefan Vogt, Sebastian Häfner, Uwe Sterr, Christian Lisdat, Heiner Denker, Christian Voigt, Ludger Timmen, Antoine Rolland *et al.*, Geodesy and metrology with a transportable optical clock, Nat. Phys. **14,** 437 (2018).

[96] Masao Takamoto, Ichiro Ushijima, Noriaki Ohmae, Toshihiro Yahagi, Kensuke Kokado, Hisaaki Shinkai, and Hidetoshi Katori, Test of general relativity by a pair

of transportable optical lattice clocks, Nat. Photonics **14**, 411 (2020).

[97] See Supplemental Material at http://link.aps.org/supplemental/10.1103/PhysRevD.108.015003 for details.

[98] Rodney Loudon, *The Quantum Theory of Light* (Oxford University Press, Oxford, New York, 2000).

[99] Bahaa Saleh, *Fundamentals of Photonics* (Wiley, Hoboken, NJ, 2019).

[100] Itay M. Bloch, Gil Ronen, Roy Shaham, Ori Katz, Tomer Volansky, and Or Katz, New constraints on axion-like dark matter using a Floquet quantum detector, Sci. Adv. **8**, eabl8919 (2022).

[101] Jae Hyeok Chang, Rouven Essig, and Samuel D. McDermott, Supernova 1987a constraints on sub-GeV dark sectors, millicharged particles, the QCD axion, and an axion-like particle, J. High Energy Phys. 09 (2018) 051.

[102] William DeRocco, Peter W. Graham, and Surjeet Rajendran, Exploring the robustness of stellar cooling constraints on light particles, Phys. Rev. D **102**, 075015 (2020).

[103] Christian Lisdat, G. Grosche, N. Quintin, C. Shi, S. M. F. Raupach, C. Grebing, D. Nicolodi, F. Stefani, A. Al-Masoudi, S. Dörscher *et al.*, A clock network for geodesy and fundamental science, Nat. Commun. **7**, 1 (2016).

[104] Marianna S. Safronova, Sergey G. Porsev, Christian Sanner, and Jun Ye, Two Clock Transitions in Neutral Yb for the Highest Sensitivity to Variations of the Fine-Structure Constant, Phys. Rev. Lett. **120**, 173001 (2018).

[105] M. G. Kozlov, M. S. Safronova, J. R. Crespo López-Urrutia, and P. O. Schmidt, Highly charged ions: Optical clocks and applications in fundamental physics, Rev. Mod. Phys. **90**, 045005 (2018).

[106] Ekkehard Peik, Thorsten Schumm, M. S. Safronova, Adriana Palffy, Johannes Weitenberg, and Peter G. Thirolf, Nuclear clocks for testing fundamental physics, Quantum Sci. Technol. **6**, 034002 (2021).

[107] Yevgeny V. Stadnik, New bounds on macroscopic scalar-field topological defects from nontransient signatures due to environmental dependence and spatial variations of the fundamental constants, Phys. Rev. D **102**, 115016 (2020).

[108] Kurt Hinterbichler and Justin Khoury, Screening Long-Range Forces through Local Symmetry Restoration, Phys. Rev. Lett. **104**, 231301 (2010).

[109] Matt Jaffe, Philipp Haslinger, Victoria Xu, Paul Hamilton, Amol Upadhye, Benjamin Elder, Justin Khoury, and Holger Müller, Testing sub-gravitational forces on atoms from a miniature in-vacuum source mass, Nat. Phys. **13**, 938 (2017).

[110] Vladimir Schkolnik, Dmitry Budker, Oliver Fartmann, Victor Flambaum, Leo Hollberg, Tigran Kalaydzhyan, Shimon Kolkowitz, Markus Krutzik, Andrew Ludlow, Nathan Newbury, Christoph Pyrlik, Laura Sinclair, Yevgeny Stadnik, Ingmari Tietje, Jun Ye, and Jason Williams, Optical atomic clock aboard an Earth-orbiting space station (OACESS): Enhancing searches for physics beyond the standard model in space, Quantum Sci. Technol. **8**, 014003 (2022).